Optical measurements of ripples using a scanning laser slope gauge Part I: Instrumentation and preliminary results

Robert J. Martinsen† and Erik J. Bock*

†Lightwave Atmospherics, Inc.
2 Susan Road
Marblehead, MA 01945

*Woods Hole Oceanographic Institution
Applied Ocean Physics & Engineering Dept.
Woods Hole, MA 02543

ABSTRACT

We describe the design, implementation, and deployment of a laser slope gauge developed at the Woods Hole Oceanographic Institution for the purpose of studying the propagation characteristics of capillary ripples, and how currents and natural slicks on the ocean surface modify ripple spectra. The laser slope gauge constitutes a nondisruptive optical technique for determining the slope spectrum for a range of waves with wavelengths between 2 mm and 20 cm using both spatial and temporal information. Operation of the sensor and data acquisition system is discussed and a sample data record collected in the Gulf Stream off Cape Hatteras, NC is interpreted and analyzed.

1. INTRODUCTION

The study of short wave propagation on the sea surface[1-5] is important for the remote sensing of subsurface currents and internal waves by identifying correlations between free surface hydrodynamics and features observed in radar imagery[6,7]. Multiple sensor measurements gathered during the Office of Naval Research-sponsored HIRES I experiment (the pilot experiment of the high resolution advanced research initiative) have led to a better understanding of how the collective effects of wind stress, current fields and surface slicks interact to produce spatially inhomogeneous ripple fields on the sea surface.

Central to the field experiment was the deployment of a scanning laser slope gauge (SLSG) that elicited information about the propagation of ripples for studying air/sea interactions and how slicks on the ocean surface modify the wave spectrum, especially at high wavenumbers[8]. The instrument was designed to be integrated with a research catamaran[9] to acquire unobstructed measurements of wave spectra and/or surface roughness as the platform is towed at a rate of 4 knots. The dynamic range of the SLSG is consistent with gathering spectral information of waves having wavelengths between 2 mm and 20 cm, with frequencies up to 64 Hz. In the mode of operation reported herein, only frequency spectra are analyzed.

The catamaran (referred to as LADAS, for *L*aser slope gauge, *A*coustic *D*oppler current profiler, *A*coustic anemometer, *S*urface sampler) is equipped with several sensors. Only partial results obtained from the SLSG and an X-band Doppler radar are reported here.

2. SENSOR DESIGN & DATA COLLECTION STRATEGY

The SLSG consists of two subassemblies, namely, a laser pod and an optical receiver. Both units were designed to be rigidly attached to a catamaran with the laser pod deployed below the waterline and the receiver above the waterline. The basic configuration is depicted in Figure 1. As the catamaran is towed through the water, the sensor unobstructively measures the local slope of the free surface. In its simplest mode of operation, the laser pod transmits a stationary vertical beam that penetrates the sea surface. In this mode, the apparent frequency spectrum of surface slope (up to 83 Hz) can be measured. In its more complex mode the laser beam is scanned to extract spatio-temporal data records for the measurement of full 3 dimensional spectra (with spatial and temporal resolution of 10.5 cm^{-1} and 395 rad s^{-1}, respectively). We will now discuss the operating principles of the SLSG and show results obtained in the apparent frequency mode.

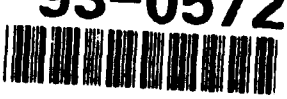

REPORT DOCUMENTATION PAGE

Form Approved
OMB No. 0704-0188

1. AGENCY USE ONLY (Leave blank)	2. REPORT DATE	3. REPORT TYPE AND DATES COVERED
	3/93	TECHNICAL

4. TITLE AND SUBTITLE
OPTICAL MEASUREMENTS OF RIPPLES USING A SCANNING LASER SLOPE GAUGE PART I: INSTRUMENTATION AND PRELIMINARY RESULTS

5. FUNDING NUMBERS
ONR N00014-90-J-1717

6. AUTHOR(S)
ROBERT J. MARTINSEN AND ERIK J. BOCK

7. PERFORMING ORGANIZATION NAME(S) AND ADDRESS(ES)
WOODS HOLE OCEANOGRAPHIC INSTITUTION
WOODS HOLE, MA 02543

8. PERFORMING ORGANIZATION REPORT NUMBER
WHOI CONTR. 8071

9. SPONSORING/MONITORING AGENCY NAME(S) AND ADDRESS(ES)
OFFICE OF NAVAL RESEARCH
ENVIRONMENTAL SCIENCES DIRECTORATE
ARLINGTON, VA 22217-5660

10. SPONSORING/MONITORING AGENCY REPORT NUMBER

11. SUPPLEMENTARY NOTES
In citing this report in a bibliography, the reference given should be: OPTICS OF THE AIR-SEA INTERFACE: THEORY AND MEASUREMENT. LELAND ESTEP, ED. SPIE - THE INTERNATIONAL SOCIETY FOR OPTICAL ENGINEERING, BELLINGHAM. 1749:258-271, 1992

12a. DISTRIBUTION/AVAILABILITY STATEMENT
APPROVED FOR PUBLIC RELEASE:
DISTRIBUTION UNLIMITED

12b. DISTRIBUTION CODE

13. ABSTRACT *(Maximum 200 words)*

We describe the design, implementation, and deployment of a laser slope gauge developed at the Woods Hole Oceanographic Institution for the purpose of studying the propagation characteristics of capillary ripples, and how currents and natural slicks on the ocean surface modify ripple spectra. The laser slope gauge constitutes a nondisruptive optical technique for determining the slope spectrum for a range of waves with wavelengths between 2 mm and 20 cm using both spatial and temporal information. Operation of the sensor and data acquisition system is discussed and a sample data record collected in the Gulf Stream off Cape Hatteras, NC is interpreted and analyzed.

14. SUBJECT TERMS
1) CAPILLARY RIPPLES
2) LASER SLOPE GAUGE
3) SLOPE SPECTRUM

15. NUMBER OF PAGES
14

16. PRICE CODE

17. SECURITY CLASSIFICATION OF REPORT	18. SECURITY CLASSIFICATION OF THIS PAGE	19. SECURITY CLASSIFICATION OF ABSTRACT	20. LIMITATION OF ABSTRACT
UNCLASSIFIED	UNCLASSIFIED	UNCLASSIFIED	

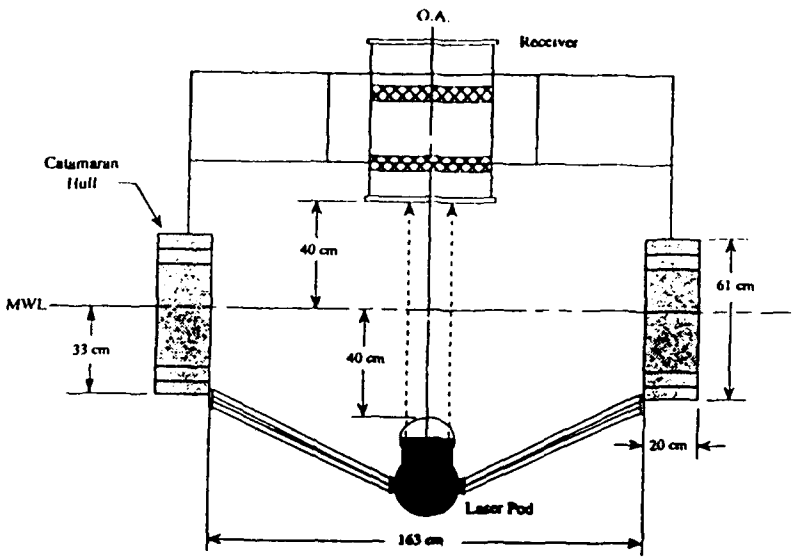

Figure 1a. Sensor configuration - front view

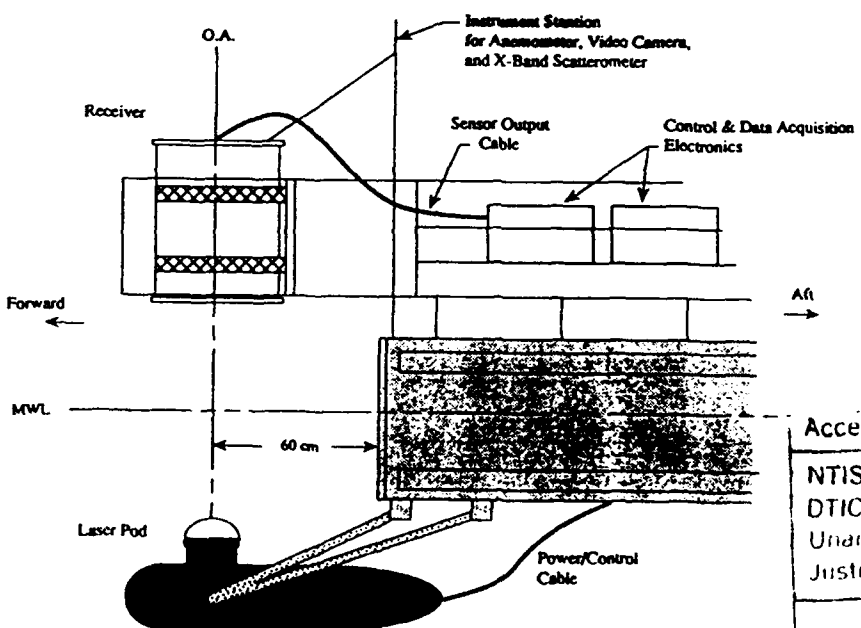

Figure 1b. Sensor configuration - side view

As illustrated in Figure 2, the beam is deflected off the optical axis by an angular amount proportional to the local slope of the free surface. The refracted beam is focused by an aspheric lens in the detector head so that its image at the focal plane is displaced proportional to that local slope. The location of this displaced beam is detected in real-time by an orthogonal set of four photodiodes in the detector. The centroiding algorithm relies on the individual measurements from each of the photodiodes to infer the angular deflection of the beam, and thus, the x and y components of surface slope. As the catamaran is towed, the collected time-series represents the variation of ripple slope with distance - which is the spatial derivative of ripple amplitude. Inertial sensors onboard the catamaran allow for the subtraction of the platform velocity to compute the wavelength of the ripples.

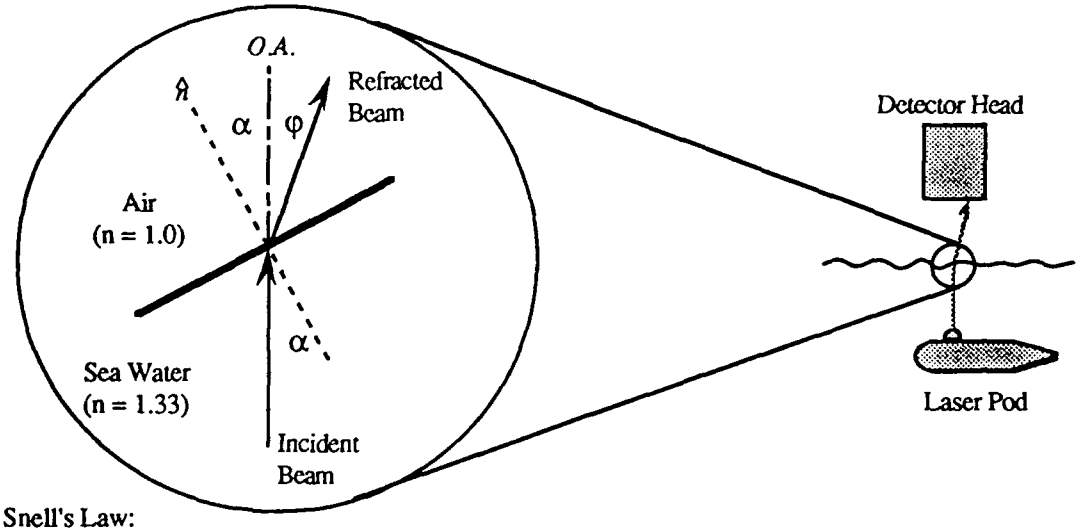

Following Snell's Law:

$\sin^{-1}(1.33 \sin\alpha) - \alpha = \varphi \quad \Longrightarrow \quad \varphi \approx 0.33\,\alpha$

Figure 2. Beam geometry at the air/sea interface

2.1 The Laser Pod

The laser pod, shown in Figure 3, contains a 10 milliwatt cw helium-neon laser, a two-axis galvo scanner, two fold mirrors, and a custom aspheric lens. All the components, except for the lens, are secured to a common tray which is attached to one of the end caps. The tray facilitates the convenience of performing the optical alignment outside of the tube, in addition to keeping the alignment intact whenever the tray is removed from the tube for diagnostic purposes.

The He-Ne laser emits a 0.8 mm diameter TEM_{00} beam measured at the $1/e^2$ irradiance points. The two-axis scanner employs two limited rotation servo motors (galvonometers) configured in an orthogonal set. Each galvo controls the movement of a small mirror to perform beam steering in the x- and y-directions. A capacitive rotation sensor in each device provides closed loop control over the angular position of the mirrors.

Beam propagation through the laser pod can be described by the following sequence of events. Fold mirror M1 redirects the light emerging from the laser by 90° up to the scanner. At the scanner, the beam strikes the x-galvo mirror first and bounces a few millimeters away to the larger y-galvo mirror. After the y-galvo mirror, the beam has been slewed in two dimensions. The resulting scan pattern is propagated down the axis of the laser pod to a large fold mirror M2 which redirects the light 90° up to the asphere lens L1. The lens collimates the scan pattern so that all off-axis rays become

parallel once they emerge from the lens. The lens forms the exit aperture of the laser pod and was designed to operate with air on one side and sea water on the other.

The laser pod's optical axis is co-aligned with the detector head so that any angular offset of the beam from a parallel ray is solely an artifact of the intervening free surface interface. After penetrating the free surface, the beam is captured by the receiver where its angular deflection is measured in terms of the spot's centroid on the horizontal x-y plane.

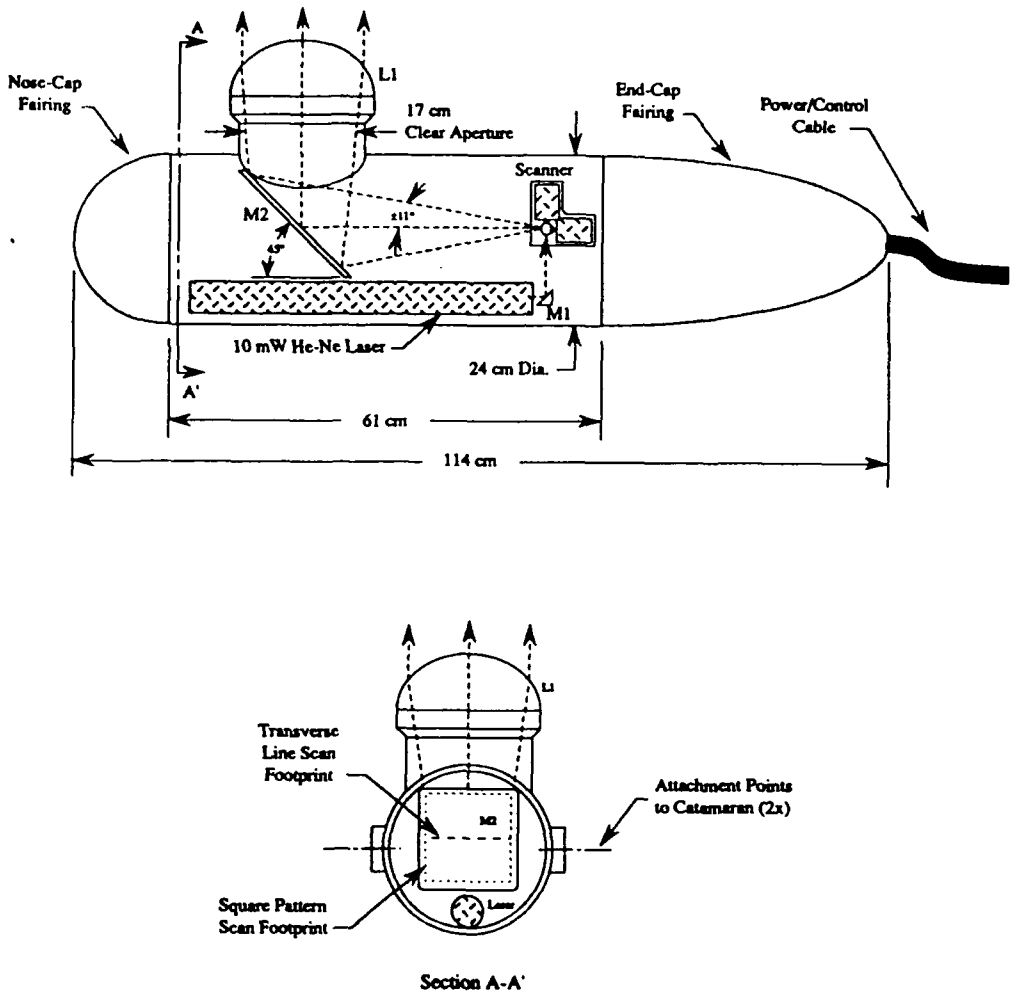

Figure 3. Opto-mechanical layout of the laser pod

2.2 The Detector Head

A schematic of the detector head is shown in Figure 4. Along the forward direction of the optical path, components in the head unit include a bandpass filter (A), a plano-convex lens (B), a diffuser plate (C), an image plane reflector plate (D), and a printed circuit board (E) containing four silicon photo-diodes with 10 nm interference filters and analog signal conditioning electronics.

The interference filters are centered about the 633 nm He-Ne line for strong ambient light rejection. The diffuser plate, positioned at the focal plane of the lens L2, acts as a quasi-Lambertian surface operating in transmission. Its purpose is to forward scatter the laser radiation into a broad Gaussian profile. Quad cell detection at a distance of 12 cm above the diffuser is used to centroid the location of the beam. The centroiding algorithm yields measurements of the x- and y-components of surface slope.

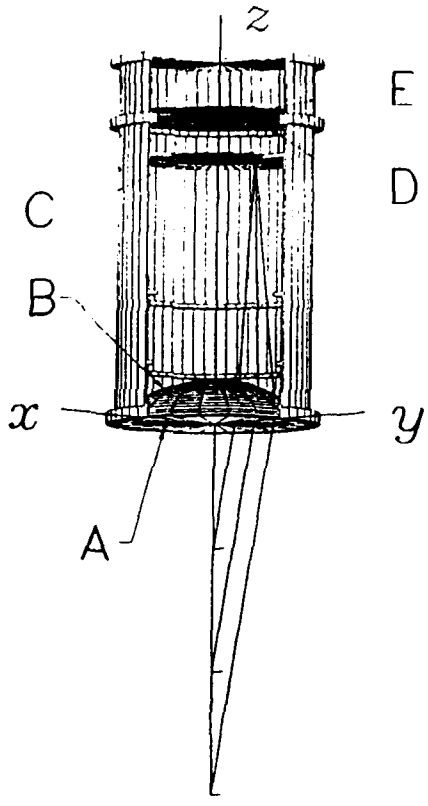

Figure 4. Schematic of the Detector Head

2.3 Sensor Control, Data Acquisition & Modes of Operation

A functional block diagram showing the electrical interfaces between the sensor, control electronics, and data acquisition system is illustrated in Figure 5. In addition to the laser pod and detector head, the overall system hardware includes:

- a General Scanning DE-2000™ scan controller which drives the galvos in the laser pod, controlled by serial line {E};
- two programmable microcontrollers [WHOI-3000's] that read n data points in response to a TTL trigger supplied by the DE-2000 via data line {D}, (the number n is a function of the sampling scheme);
- a 25 MHz 386 computer with two Metrabyte PIO-12 parallel I/O cards, a 3COM Ethernet adapter, and serial port;
- a DEC 5000 computer on the Ethernet line {G};
- a Compaq portable on the serial lines {E} and {F}.

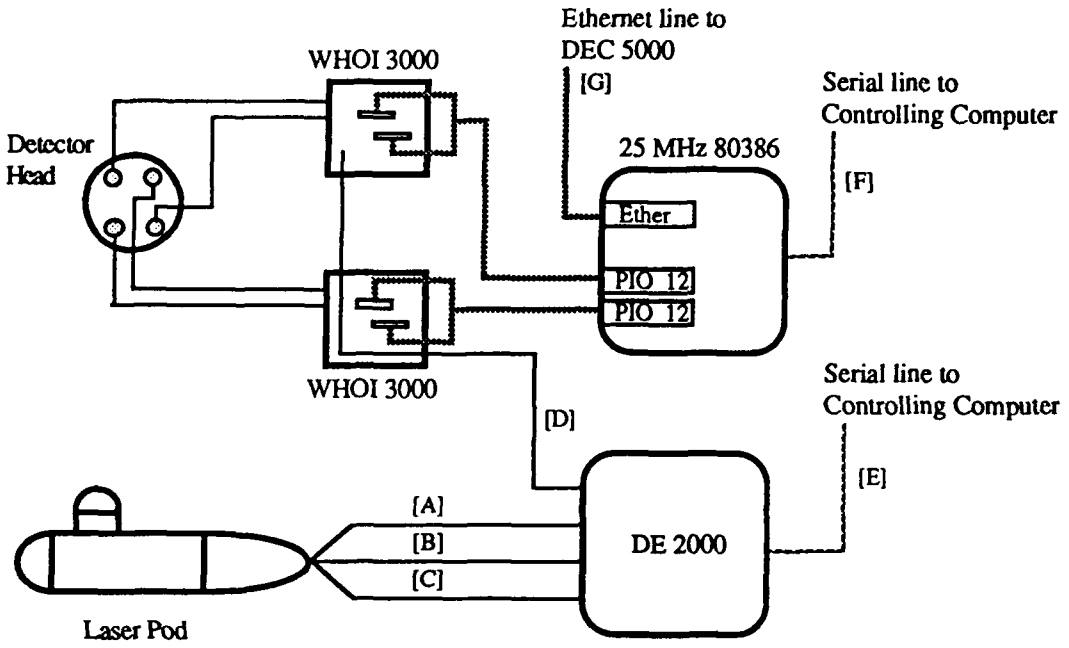

Figure 5. Functional block diagram of the sensor system

The 386 receives messages at the serial line to initiate sampling. Data collection activity proceeds until another message requests the 386 to stop sampling. The DE-2000 is programmed to execute scan sequences for spatio-temporal sampling and non-scanning modes. During the square pattern sampling mode, the scanner writes out a square with 10 cm sides. At the start of each square, the DE-2000 emits a TTL pulse. The WHOI-3000's then begin A/D conversions and each WHOI-3000 samples a light intensity value corresponding to its respective x- or y-channel. Each will accumulate 129 pairs of readings in about 10 ms. This corresponds to 32 pairs per side of the square. Each pair represents the light intensities at the two photodiodes for one component of slope.

3. DATA ANALYSIS

In this Section, a sample time series of 2-D surface slope acquired by the laser slope gauge is analyzed. The statistical and spectral properties of the surface slope data are related to sensor parameters and the efficacy of the sensor to measure ocean surface roughness is discussed. First, we begin with a description of the pre-processing performed on the stored data to prepare it for data analysis.

3.1 Pre-processing of the Raw Data

The spot position on the image plane as a function of time was constructed using the four-channel time-series of intensities. The (x,y) coordinates of the spot position were calculated using a component-pair centroiding algorithm:

$$x = \left(\frac{A - B}{A + B}\right) \quad \Rightarrow \quad \text{fore / aft coordinate}$$

$$y = \left(\frac{C - D}{C + D}\right) \quad \Rightarrow \quad \text{transverse coordinate}$$

which produces a normalized position in the local coordinates of the image plane with limits $-1 \le x \le 1$ and $-1 \le y \le 1$, as illustrated in Figure 7. When the intensities at the four detectors are equal, the computed centroid of the spot is (0,0), i.e. the spot is aligned with the optical axis, corresponding to a zero surface slope condition. Given the geometry of the

refracted beam (see Figure 2) and the optical ray trace of the head unit (see Figure 4), the position of the spot on the image plane is directly related to the local inclination of the sea surface. For small angles (≤ 13 degrees) of beam deflection, the spot position on the image plane is related to the surface slope in the x- and y-directions by the relationship:

$$\alpha_x \approx 3 \tan^{-1}(Cx) \quad ==> \quad \text{fore/aft surface slope}$$

$$\alpha_y \approx 3 \tan^{-1}(Cy) \quad ==> \quad \text{transverse surface slope}$$

where C is a constant defined by the ratio of the spatial separation of the detectors, ζ, from the optical axis and the focal length, f, of the lens in the receiver. For our system, $\zeta = 8.85$ cm and $f = 43.18$ cm which makes $C = 0.205$. Hence, the laser slope gauge is capable of measuring surface slopes of $\pm 34.8°$.

Upon completion of the pre-processing, three time-series are generated from the raw data:

- Four channels of detector intensities I_A, I_B, I_C and I_D;
- Centroided spot position (x,y) on the image plane;
- 2-D surface slope α_x and α_y.

The detector intensities take on values between 0 and 1023 as a result of our 10-bit A/D conversion, and the normalized spot position and surface slope have the limits $-1 \le x,y \le +1$ and $-35° \le \alpha_{x,y} \le +35°$, respectively.

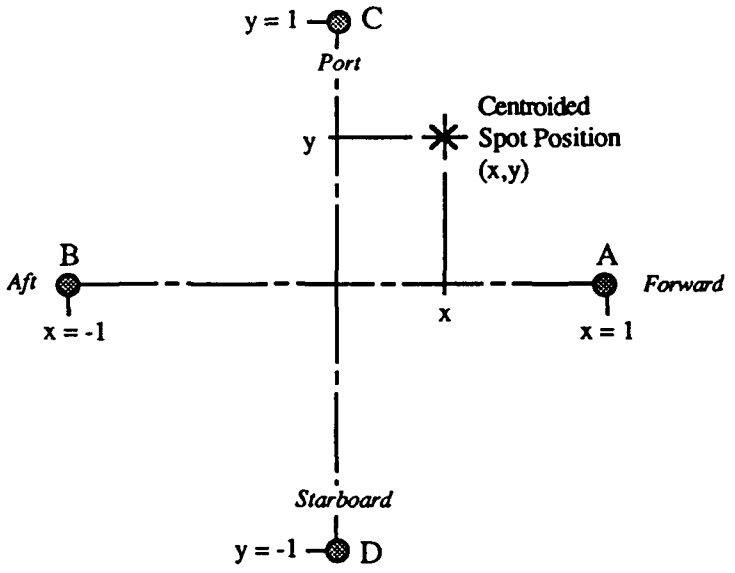

Figure 7. Normalized spot position on the image plane

3.2 Description of the HIRES I Data Record

During the HIRES I field experiment off the coast of Cape Hatteras, the laser slope gauge was operated in the non-scanning mode for the measurement of ocean surface roughness. The data record reported here was collected on the 16th of September beginning at 10:09 AM local time and lasts for approximately 10 minutes. According to the ship's log and data acquired by other sensors, the laser slope gauge data should contain features associated with a current-field boundary. Based on satellite thermal imagery, it is believed that this current field may be associated with an eddy along the western edge of the Gulf Stream.

The catamaran was being towed at 4 knots (≈ 2 m/s) and data was sampled at 167 Hz. Given this tow velocity and sampling rate, the platform was translated approximately 1.2 cm between samples. The spatial resolution of the sensor is governed by the 1 mm diameter of the laser beam.

It is important to note here that the measurements are somewhat difficult to interpret owing to their mixed temporal and spatial nature. For a fixed laser slope gauge, time-series measurements can be analyzed by Fast Fourier Transforms (FFT) to produce frequency spectra. For a scanning laser slope gauge, FFT analysis directly yields wavenumber spectra. The measurements obtained in the September field experiment are a hybrid of these techniques due to the fact that the fixed laser was translated at about 2 m/s. This rate is large enough so that some waves (those with phase velocities less than 2 m/s) were overtaken by the gauge, and others were not. This has the effect of aliasing waves into improper frequency (or wavenumber) bins. To avoid errors resulting from this effect, the analysis described below should not be taken to literally represent either frequency or wavenumber spectra. It is intended to represent surface roughness via the frequency representation of slope variance.

3.3 Statistical Analysis

Evaluating the statistical properties of the sample data record reveals important information about the performance of the sensor. Parameters such as sensor bias, dynamic range, and scale factor, for example, can be estimated from the computed mean, standard deviation, and covariance of the detector intensity and spot position time-series.

If the laser pod and detector head were perfectly aligned and the responsivity of the detectors were equal, we would expect identical values of mean detector intensity over the 10 minute data record for the four optical channels, i.e.

$$\bar{I}_A = \bar{I}_B = \bar{I}_C = \bar{I}_D$$

In practice, however, this is rarely the case. At the time this data was collected, the mean values of detector intensity were

$$\bar{I}_A = 430 \qquad \bar{I}_C = 470$$
$$\bar{I}_B = 449 \qquad \bar{I}_D = 431$$

which yields a mean centroided spot position in the normalized coordinate frame of

$$\bar{x} = -4.165 \times 10^{-2}$$

$$\bar{y} = 6.067 \times 10^{-2}$$

corresponding to a surface slope bias of

$$\bar{\alpha}_x = -1.47^\circ$$

$$\bar{\alpha}_y = 2.14^\circ$$

This surface slope bias is related to the cumulative errors of both nonuniform responsivity and optical misalignment, resulting in an effective off set from the optical axis given by

$$r = \sqrt{(\bar{x})^2 + (\bar{y})^2}$$

$$= .074$$

where r is the radial distance away from the optical axis, in the normalized coordinate frame, whose real distance is

$$R = r\,\zeta$$

$$= .65 \text{ cm}$$

The effective origin of the image plane is therefore 6.5 mm aft and to port of the real optical axis. This brings asymmetry to the dynamic range of our sensor. Rather than having the design measurement limits of ±34.8° in x and y surface slope, we instead have $[-33.3°, +36.2°]_x$ and $[-36.9°, +32.6°]_y$. An adjustment to our scale factor can be made that accounts for the bias.

$$\alpha_x' = 1.47 + [3 \tan^{-1} (.205x)] \quad ==> \quad \text{fore / aft surface slope}$$

$$\alpha_y' = -2.14 + [3 \tan^{-1} (.205y)] \quad ==> \quad \text{transverse surface slope}$$

The covariance of the spot coordinates σ^2_{xy} also serves as a useful diagnostic. Figure 8 is a scatter plot in $\sigma_x : \sigma_y$ space with a 2σ covariance ellipsoid superposed on the data. Each point on this plot corresponds to the standard deviation in the x- and y-spot coordinates simultaneously computed over 1 second intervals containing 167 samples.

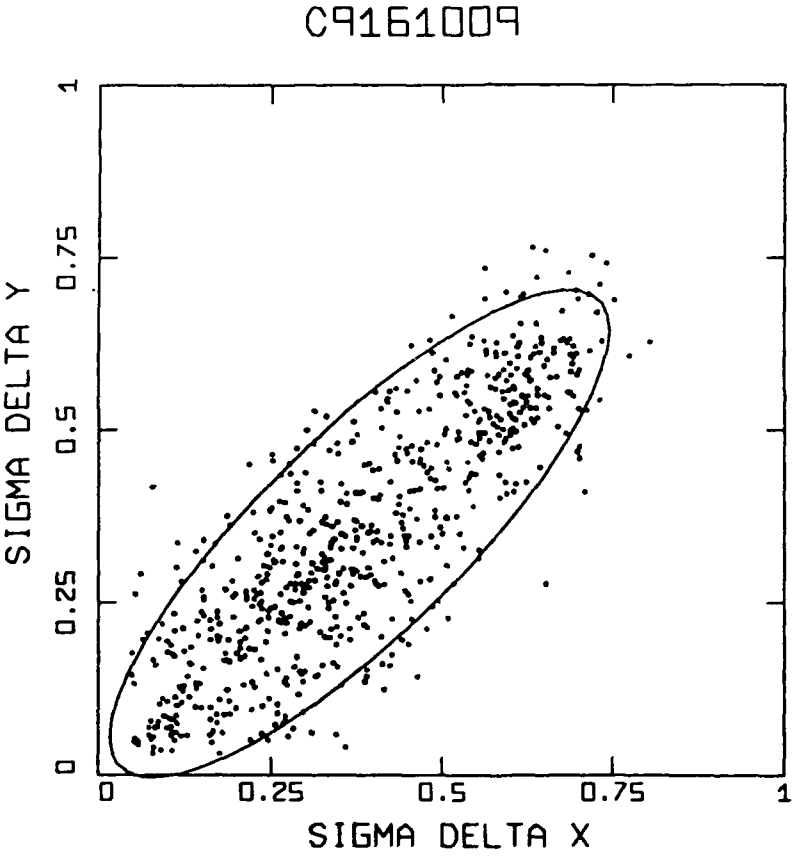

Figure 8. Covariance of the x,y spot coordinates on the image plane

Since the standard deviation of spot position is related to the magnitude of surface roughness, the +45° orientation of the ellipsoid is expected for these positively correlated parameters. In other words, when high surface roughness is encountered along the x-axis, high surface roughness should (on average) be encountered along the y-axis as well. In the limit of a perfectly correlated distribution, the ellipsoid would collapse to a line. Due to the nature of the process and measurement scheme we do not anticipate a perfectly correlated distribution in $\sigma_x : \sigma_y$ space. What we do expect, however, is a smooth distribution of the covariance without abrupt transitions or evidence of multimodal behavior. The laser slope gauge does indeed exhibit this smoothness as witnessed in Figure 8.

As a first-cut procedure for scanning the data for surface roughness features, it is convenient to plot $\sigma_x(t)$ and $\sigma_y(t)$. Figure 9 shows such a plot for the time interval of $400 \leq t \leq 500$ seconds. The standard deviations σ_x and σ_y were computed in the same manner as the results of Figure 8, i.e. at 1 second intervals using 167 samples.

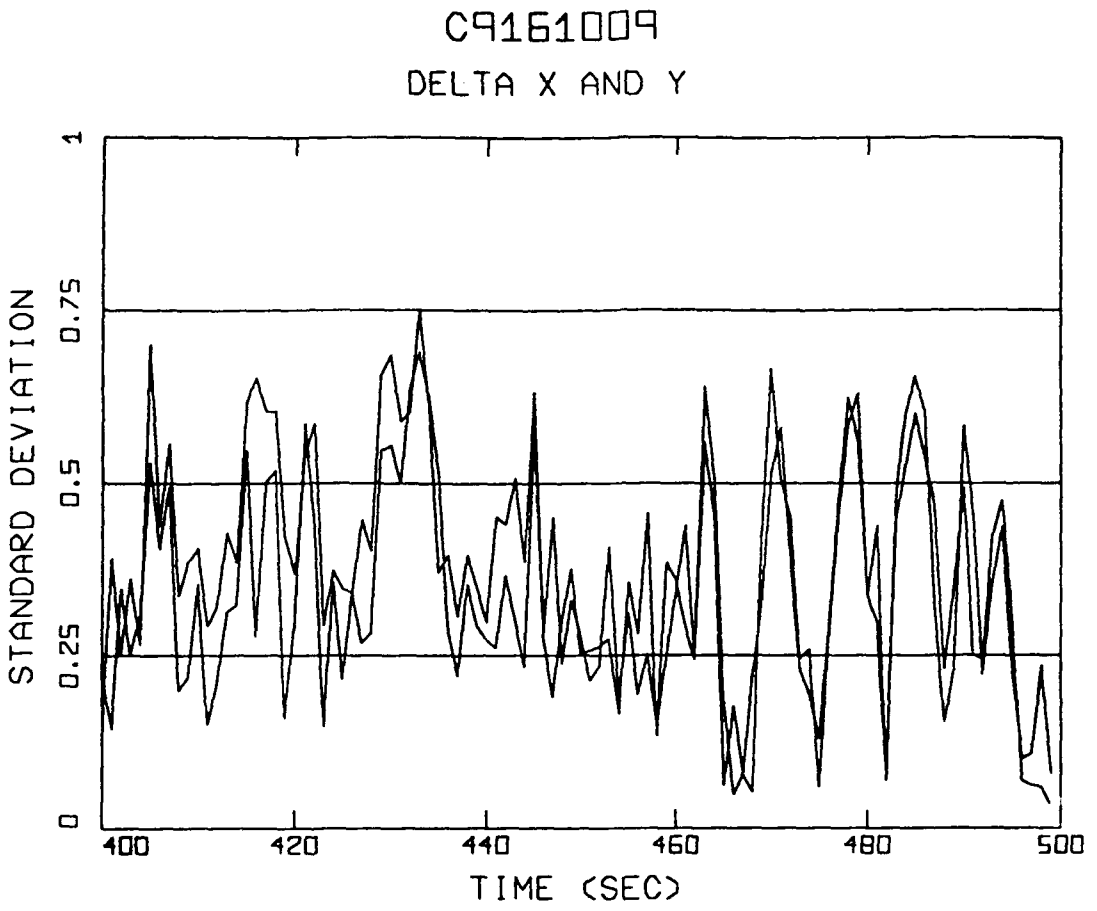

Figure 9. Time-history of the x- and y-spot coordinate standard deviations

Figure 9 contains three distinct features, namely, a wide lobe of high σ_x and σ_y centered near t = 430 sec, a region of relatively low σ_x and σ_y lasting for 15 seconds around t = 450 sec, followed by a strong and highly correlated modulation beginning at t = 460 sec and lasting for 35 seconds. Based on our tow velocity of 4 knots, these three features have a spatial extent [in the direction of platform heading] of 1.6 meters, 2.4 meters, and 7.0 meters, respectively. The period of the modulating feature starts out at approximately 8 seconds and then "bunches" towards a 2 second period before diminishing. The physical interpretation of this feature may be related to bands of roughness, which will be explored further in Section 3.4.

3.4 Spectral Analysis

In this section, short-time Fourier transform (STFT) representations of the sample data record are presented to characterize the change in frequency content of the surface roughness over time as the catamaran is towed through the water. Attention will be focused on the region of data suspected of containing peculiar surface features found by statistical methods. The sensor's ability to detect and quantify roughness variations on the sea surface are addressed by reviewing video and radar backscatter data collected over the same time domain.

The underlying idea for the STFT is to take a discrete Fourier transform (DFT) in the neighborhood of each time sample of our sequence. The resulting STFT representation will be related to both the time- and frequency-domain properties of the observed surface roughness. The signal processing techniques employed are an extension of the basic Fourier transform concepts for a discrete-time sequence x(n). The discrete STFT of x(n) is defined by the expression[10]

$$X(n,k) = \sum_{m=-\infty}^{m=\infty} x(m)\, w(n-m)\, e^{-j2\pi km/N}$$

where n and k are discrete variables denoting time and frequency, respectively, w(n - m) is the analysis window, and N is the frequency sampling factor.

Figure 10 gives the STFT result obtained with a 64-point Hamming window with double zero padding. The plotted result has a linear frequency scale of 0 - 83 Hz (increasing frequency to the left), and is associated with the time interval $380 \le t \le 440$ seconds (increasing time is from front to back). Thresholding was applied for suppression of background noise. No additional information of substance was revealed from the use of a 128-point window except the realization that the data is very wide band.

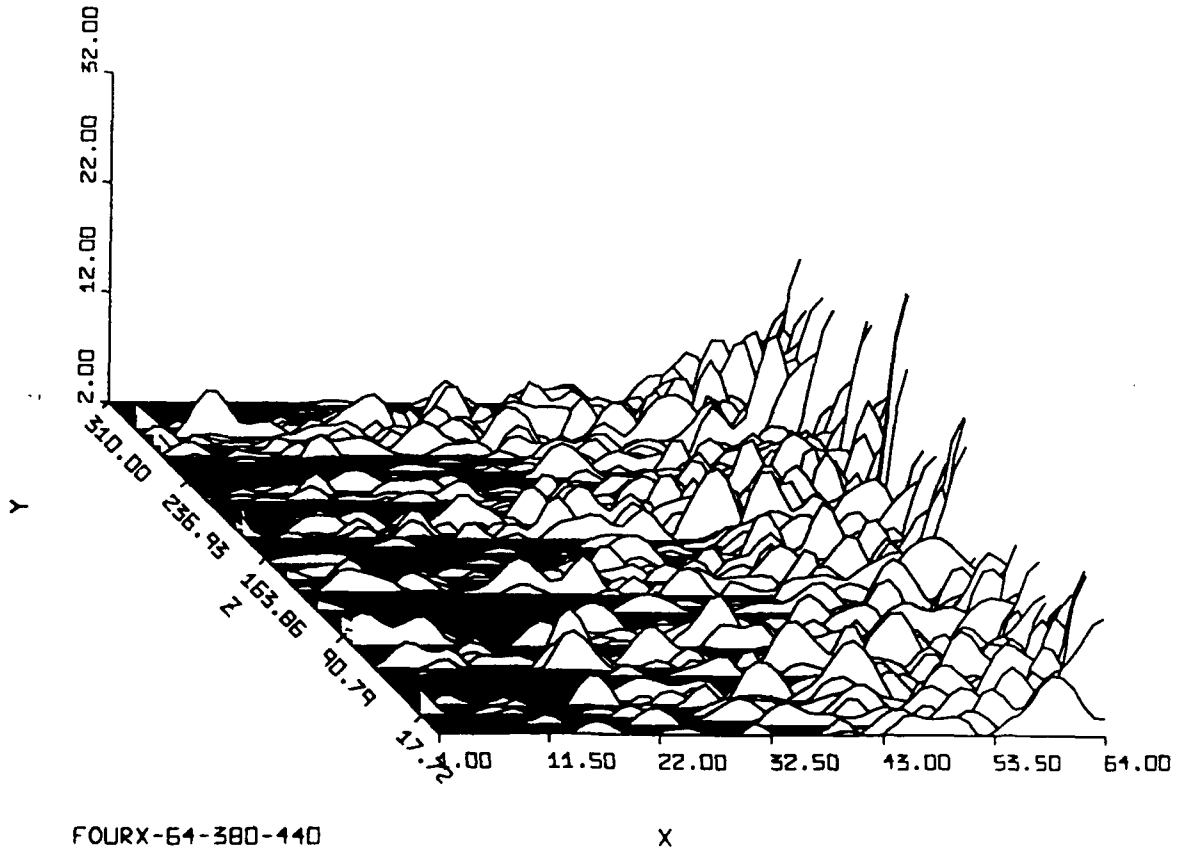

Figure 10. STFT result using a 64-point Hamming window

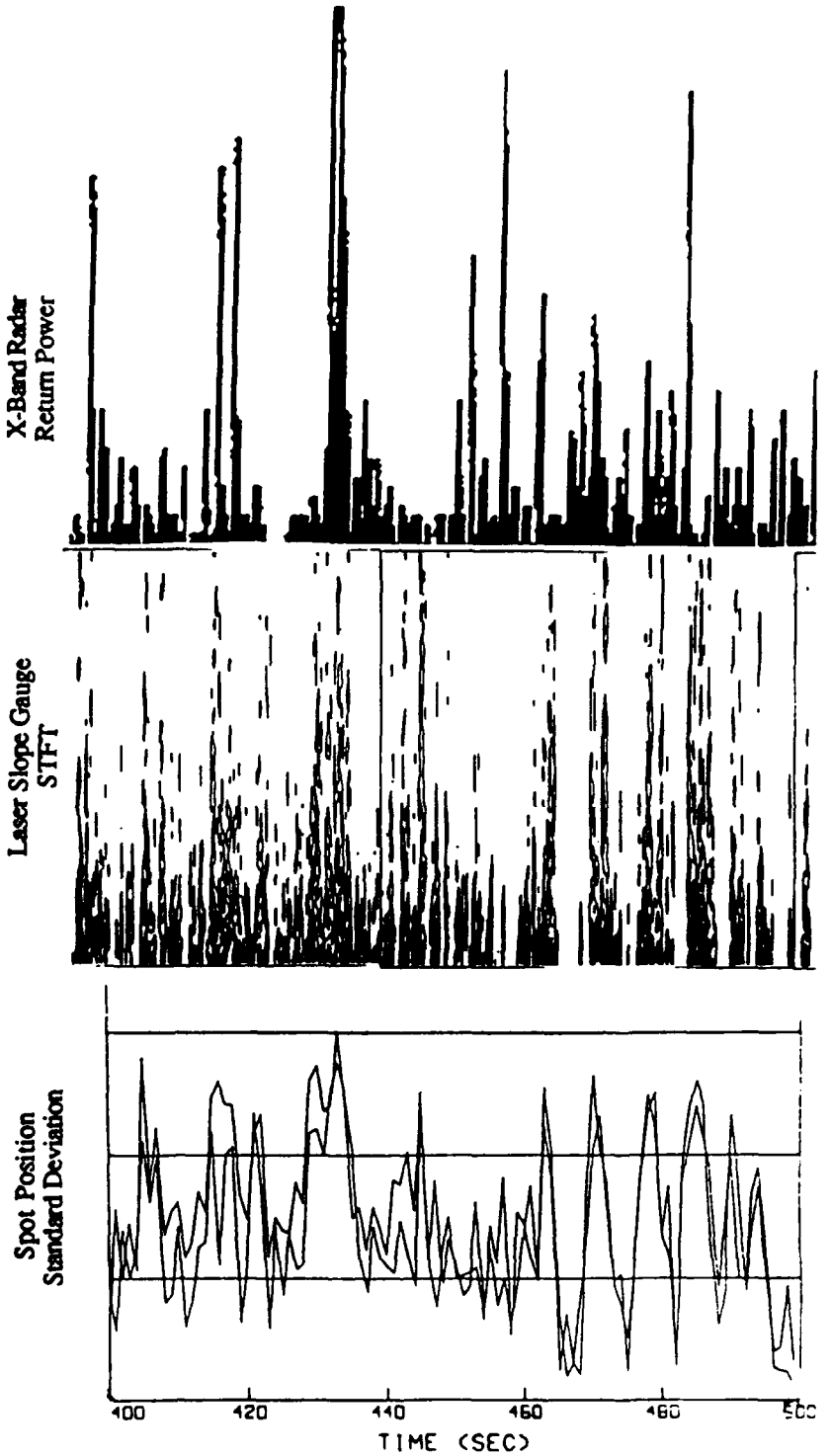

Figure 11 Comparison of STFT with spot coordinate standard deviation and X-band Doppler radar time-series

Figure 11 shows a comparison of the STFT (contour plot) with the time-history of standard deviation and X-band Doppler radar return power over the time frame $380 \leq t \leq 560$ seconds. The X-band Doppler measurements were made independently from a mast-mounted Doppler scatterometer operated by Dr. David Lyzenga of ERIM. X-band Doppler return power is proportional to surface roughness and thus serves as an independent measurement of roughness. Perfect agreement, however, is not expected because of two reasons:

1) backscatter power is a strong function of angle of incidence and the catamaran is constantly undergoing pitching motions (because the scatterometer was not mounted on a stabilized platform, angular fluctuations due to pitch directly affect angle of incidence), and

2) the measurement regions of the radar and laser slope gauge are physically separated from each other (by 5 m spatially, and 2.5 seconds temporally) and therefore some surface features detected by one sensor are not necessarily detected by the other.

A reasonable correlation exists between the STFT and the X-band radar data. This correlation suggests the existence of some features that appear on the surface long enough so as to be recorded by both sensors. These features might include wind-stress induced surface roughness or current boundary surface expressions. A strong correlation exists between features observed in the STFT and standard deviation plots. This is to be expected since the STFT surface, if integrated along the frequency axis, yields the mean-square-slope, a quantity akin to the standard deviation as defined and computed above.

The correlation between the STFT, standard deviation, and video signal is less quantifiable since the video is unprocessed. All that can be assessed is the presence (or absence) of specular reflections from facets on the sea surface. Modulations, or occurrences of alternately rough and smooth surfaces, were evident throughout the video for the times analyzed above.

4. CONCLUSION

The Laser Slope Gauge was successful in measuring surface roughness over a variety of sea-state conditions during the HIRES I field experiment off the coast of North Carolina. The sensor was operated exclusively in a non-scanning mode for the purpose of understanding the modification of surface roughness in the presence of current field boundaries and surface water temperature fronts. The utility of the LADAS catamaran to perform "ground truthing" for airborne radar platforms was also demonstrated during the experiment.

Data sets collected by the Laser Slope Gauge have been processed and analyzed in conjunction with data acquired by the other sensors on the LADAS catamaran. The processing procedures included: 1) centroiding the spot position on the image plane and 2) statistical and spectral analysis to determine instrument bias and dynamic range. The collected data has been compared in both a single-dimensional format (*e.g.* standard deviation as a function of time) and in a multi-dimensional representation (*e.g.* STFT , in both time and frequency) to independent measurements of surface roughness.

The sensor's scanning mode of operation has been tested in the laboratory and used for the first time in the field during an experiment in May of 1992 off the Massachusetts coast in Martha's Vineyard Sound. One of the major thrusts of this experiment was to gather directional spectra [i.e. $S(k_x, k_y, \omega)$] of capillary-gravity waves in the presence of natural slicks.

5. ACKNOWLEDGMENTS

This work was performed at the Woods Hole Oceanographic Institution where Mr. Martinsen was conducting graduate research for the Department of Ocean Engineering at MIT. Support for this work was provided in part by an MIT scholarship from the Gibbs Brothers Foundation and a grant from the Office of Naval Research (Grant N00014-90-J-1717). The authors would like to express appreciation to Mr. Charles Plum for unpacking the raw sensor data, writing the data analysis software, and providing the plots presented in Figures 8, 9 and 10. The authors are also thankful to Dr. David Lyzenga from ERIM for providing the X-band Doppler radar data presented in Figure 11.

6. REFERENCES

[1] Lucassen-Reynders, E.H. and Lucassen, J., "Properties of Capillary Waves", *Advances in Colloid and Interface Science*, **2**, 347-395, 1969.

[2] Bock, E.J. and Mann, J.A., Jr., " On Ripple Dynamics II. 'A Corrected Dispersion Relation for Surface Waves in the Presence of Surface Elasticity'", *Journal of Colloid and Interface Science*, **129(2)**, 501-505, 1989.

[3] Alpers, W., and Huhnerfuss, H., The Damping of Ocean Waves by Surface Films: A New Look at an Old Problem, *J. Geophys. Res.*, **94(C2)**, 6251-6265, 1989.

[4] Hansen, R.S. and Mann J.A. Jr., Propagation Characteristics of Capillary Ripples, I, The Theory of Velocity Dispersion and Amplitude Attenuation of Plane Capillary Waves on Viscoelastic Films, *J. Applied Physics*, **35**, 152-161, 1964.

[5] Herr, F.L. and Williams, J., Role of Surfactant Films on the Interfacial Properties of the Sea-Surface, *ONRL Workshop Proceedings*, **Rep. C-11-86**, Office of Naval Research, London, p. 283, 1986.

[6] Huhnerfuss, H., Alpers, W., Cross, A., Garrett, W.D., Keller, W.C., Lange, P.A., Plant, W.J., Schlude, F., Schuler, D.L., The Modification of X-Band and L-Band Radar Signals by Monomolecular Sea Slicks, *J. Geophys. Res.*, 88(2), 9817-9822, 1983.

[7] Lombardini, P.P., Fiscella, B., Trivero, P., Cappa, C., Garrett, W.D., Modulation of the Spectra of Short Gravity Waves by Sea Surface Films: Slick Detection and Characterization with a Microwave Probe, *J. Atmos. Oceanic Technol.*, **6**, 882-890, 1989.

[8] Martinsen, R.J., Optical Characterization of Oceanic Capillary-Gravity Wave Spectra, *M.S. Thesis*, Massachusetts Institute of Technology, 1991.

[9] Carlson, D.J., Cantey, J.L., Cullen, J.J., Descriptions and Results From A New Surface Microlayer Sampling Device, *Deep-Sea Res.*, **35**, 1205-1213, 1988.

[10] Nawab, S.H., and Quatieri, T.F., Short-Time Fourier Transforms, *Advanced Topics in Signal Processing*, (ed. J.S. Lim & A.V. Oppenheim), Prentice-Hall, Englewood Cliffs, NJ, 1988, 289-337.